Stress distribution in static two dimensional granular model media in the absence of friction

S. Luding
Institute for Computer Applications 1, Pfaffenwaldring 27, 70569 Stuttgart, GERMANY
e-mail: lui@ica1.uni-stuttgart.de
(to appear in Phys. Rev. E, April 1997)

We present simulations of static model sandpiles in two dimensions (2D) and focus on the stress distribution in such arrays made of discrete particles. We use the simplest possible model, i.e. spherical particles with a linear spring and a linear dashpot active on contact and without any frictional forces. Our model is able to reproduce several recent theoretical predictions. For different boundary conditions we examine the contact network and the stresses in the array and at the bottom of the pile. In some cases we observe a dip, i.e. the relative minimum in pressure, under the center of the pile. We connect the dip to arching, and we relate arching to the structure of the contact network. Finally, we find that small polydispersity is sufficient to cause a so called stress-network, i.e. strong fluctuations in stress. From these data we determine the probability distribution for the vertical stress at the bottom and relate it to theoretical and other numerical work.
PACS numbers: 46.10.+z, 05.40.+j, 83.70.Fn, 01.55.+b

I. INTRODUCTION

In recent years the physics of granular materials has received growing interest [1]. One of the many interesting features of granulates is the stress distribution in static or quasi-static arrays. In contrast to a liquid, the pressure in a silo, filled with e.g. grains, is not increasing linearly with depth, but saturates at a certain value [2]. This is due to internal friction and due to arching, so that the walls of the silo carry a part of the materials' weight. In sandpiles no walls are present so that the situation may be different, i.e. the total weight of the pile has to be carried by the bottom. However, the distribution of forces under and also inside the pile is not yet completely understood. Experiments on rather large piles show that the normal force has a relative minimum under the top of the pile, the so-called dip [3,4]. On a much smaller scale, the stress chains are observed, i.e. stresses are mainly transported along selected paths and the probability distribution of stress spans orders of magnitude [5–7].

One simple model pile is an array of rigid spheres, arranged on a diamond lattice, i.e. with four nearest neighbors each [8,9]. The force under such a pile is constant in contrast to the experimental observations, and also periodic vacancies in such a configuration do not lead to a dip in the pressure at the bottom [10]. The variation of the size of some of the particles or an attractive force between the particles may lead to a non-constant force under the pile [11]. Continuum approaches [12–16] may lead to a dip in the vertical stress if the correct assumptions for the constitutive equations are chosen. Edwards [12] introduced the notion that a pressure minimum can result from compressive stresses aligning in fixed

directions. Wittmer et al. [15,16] embellished this idea recently with concrete calculations in agreement with the experimental data [4]. A lattice model based on a random opening of contacts [17] also shows the dip in average over many realizations.

In this study we focus on 2D-situations, with particles on an almost regular lattice, which we analyse using MD-simulations. The aim is to find the dip under conditions as simple as possible and to understand the stress networks and arches. We describe the simulation method used in Sec. II and discuss the physics of particle contacts in Sec. III. The results are presented in Sec. IV and are discussed in Sec. V.

II. SIMULATION ASPECTS

The elementary units of granular materials are solid "mesoscopic" grains, interacting on contact. The surface is in general rough on a microscopic scale and solid friction is usually found. Here, we focus on properties of granular systems in the absence of friction. We will examine in how far phenomena like stress chains and arching depend on friction by neglecting solid friction. However, we have some kind of "geometrical friction", since the particles restrict the motion of their neighbors due to excluded volume effects.

Without friction, energy may still be dissipated by e.g. viscous deformations, modelled here by a simple viscous dashpot, active during the contact.

Since we are interested in static arrangements of particles in the gravitational field, we use strong viscous damping, in order to reach the steady state quickly. For the relaxation of the array we use a molecular dynamics (MD) procedure [18,19], in order to allow contacts to break. The MD method is not the best choice for a fast relaxation, but closing and opening of contacts is implemented straightforwardly.

A. Initial and Boundary Conditions

In the simulations N spherical particles, with diameters d_i, (i = 1,...,N) are used. If not explicitly mentioned we use monodisperse spheres of diameter $d_i = d_0 = 1.5$mm. The N particles are placed into a container with different boundary conditions at the bottom and also different system sizes. Starting from a regular close-packed triangular arrangement with L particles in the lowermost layer $M = 0$ at the bottom, we model heaps of slope 60^o or 30^o by adding $L_M = L - M$ or $L_M = L - 3M$ particles for layer M respectively. The number of particles is thus $N^{(60)} = H^{(60)}(L+1)/2$ or $N^{(30)} = H^{(30)}(L-3(H^{(30)}-1)/2)$ with the number of layers $H^{(60)} = L$ or $H^{(30)} = \text{int}[(L-1)/3] + 1$. The largest pile we simulate has $L = 100$ and thus $N^{(30)} = 1717$.

The initial velocities and overlaps of the particles are set to zero if not explicitly given, gravity is slowly tuned from zero to the selected magnitude and the system is simulated until the kinetic energy is several orders of magnutide smaller than the potential energy, and the stresses no longer vary. The particles at the bottom layer $M = 0$ are either fixed, or may slide horizontally and penetrate the bottom vertically. In the sliding case, only the outermost particles are fixed in horizontal direction by the sidewalls. For a schematic drawing of the four possible situations see Fig. 1(a). The pos-

sible configurations of a regular contact network are schematically drawn in Fig. 1(b).

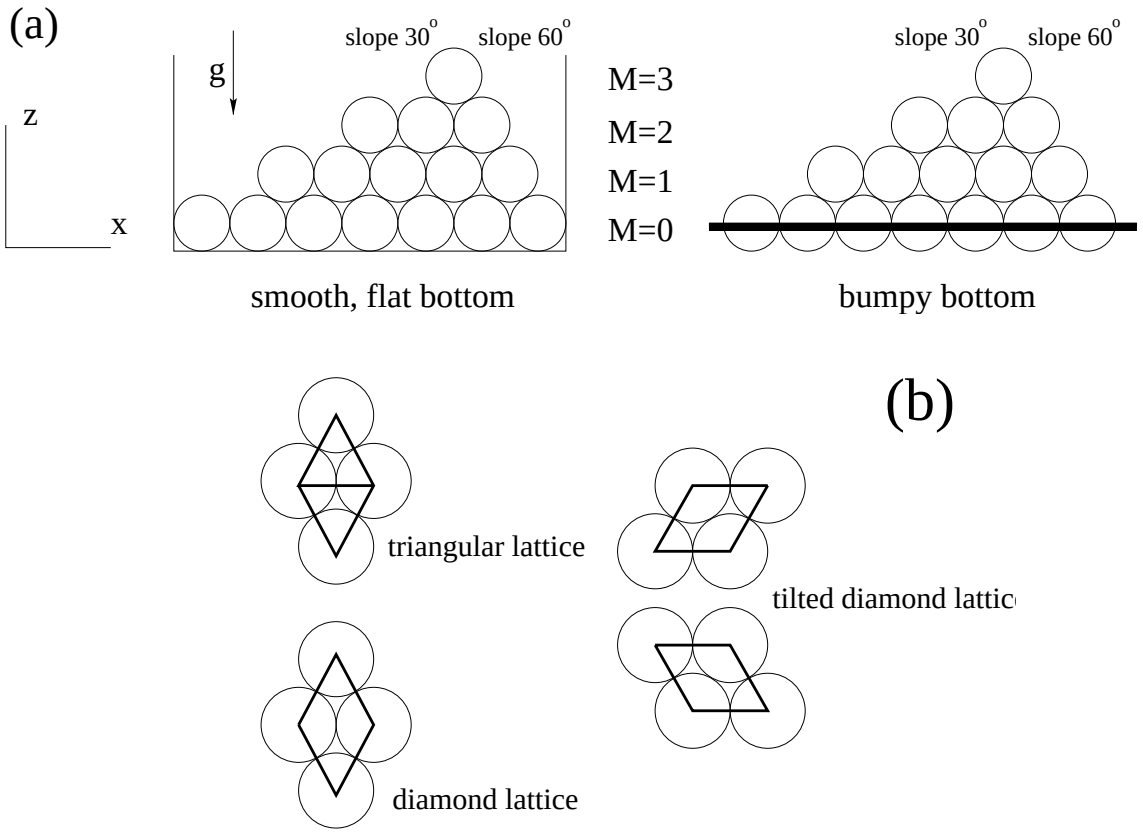

FIG. 1. (a) Schematic drawing of a pile in a box with smooth, flat bottom (left), and on a bumpy bottom (right), with $L_0 = 7$. The solid bar at the right indicates that the particles in row $M = 0$ are fixed, so that the first relevant row with mobile particles is $M = 1$ with here $L_1 = 5$. (b) Schematic drawing of the typical contact network configurations in a regular arrangement.

B. Molecular Dynamics Method

For the integration of the equations of motion we use a fifth order predictor-corrector MD-scheme, see Ref. [18,19]. Since we are interested in a static situation in 2D, with almost monodisperse particles, no particle has more than six nearest neighbors. For the simulation we keep the neighbors in memory in order to reduce the computational effort.

There are two forces acting on particle i when it overlaps with particle j, i.e. when the distance $r_{ij} = \mid \vec{r}_j - \vec{r}_i \mid \leq (d_i + d_j)/2$. We use an elastic force

$$\vec{f}_{el}^{(i)} = k(r_{ij} - \frac{1}{2}(d_i + d_j))\vec{n}_{ij}, \tag{1}$$

with the spring constant k, acting on particle i in normal direction $\vec{n}_{ij} = (\vec{r}_j - \vec{r}_i)/r_{ij}$. The second force in normal direction is dissipative

$$\vec{f}_{diss}^{(i)} = \mu(\vec{v}_{ij} \cdot \vec{n}_{ij})\vec{n}_{ij}, \tag{2}$$

accounting for the inelasticity of the contacts. In Eq. 2 the constant μ is a phenomenological dissipation coefficient, and $\vec{v}_{ij} = \vec{v}_j - \vec{v}_i$ is the relative velocity of the particles i and j. As mentioned above, we neglect tangential forces. The contact of a particle with a wall or an immobile particle is mimicked by setting the mass of the immobile contact partner to infinity. Finally, the influence of gravity g is readily included into the equations of motion.

III. CONTACTS

Now we are interested in the static limit, where particles ideally have zero relative velocities and are either in contact or separated by a gap and in the latter case do not interact. However, we will discuss in this section the dynamics of contacts in order to estimate the typical scales of the system.

A. Two particle contacts

Since we use no tangential forces, we will discuss the normal direction of a contact only. Considering the collision of two particles, the situation is modelled by a spring and a dashpot, see Eqs. 1 and 2 so that the relative acceleration during contact is $y'' = (d^2/dt^2)r_{ij} = f^{(j)}/m_j - f^{(i)}/m_i$, with $f^{(i)} = f^{(i)}_{el} + f^{(i)}_{diss}$. Due to force balance we set $f^{(j)} = -f^{(i)}$ what leads to a differential equation for negative penetration depth $y = r_{ij} - (1/2)(d_i + d_j)$:

$$y'' \; + \; 2\gamma y' \; + \; \omega_0^2 y \; = \; 0. \tag{3}$$

In Eq. 3, $\omega_0 = \sqrt{k/m_{ij}}$, $\gamma = \mu/(2m_{ij})$, and the reduced mass $m_{ij} = m_i m_j/(m_i + m_j)$. The solution of Eq. 3 is for $y \leq 0$:

$$y(t) \; = \; (v_0/\omega) \;\; \exp(-\gamma t) \;\; \sin(\omega t), \tag{4}$$

with the corresponding velocity:

$$y'(t) \; = \; (v_0/\omega) \;\; \exp(-\gamma t) \;\; [-\gamma \;\; \sin(\omega t) + \omega \;\; \cos(\omega t) \;]\,. \tag{5}$$

In Eqs. 4 and 5 $v_0 = y'(0)$ is the relative velocity before collision and $\omega = \sqrt{\omega_0^2 - \gamma^2}$ the damped frequency. As long as $\gamma^2 < \omega_0^2$, the typical duration of the contact of two particles is:

$$t_c = \pi/\omega, \tag{6}$$

because the interaction ends when $y(t) > 0$. The coefficient of restitution ϵ is defined as the ratio of velocities after and before contact $\epsilon = -y'(t_c)/y'(0)$ so that Eqs. 5 and 6 lead to

$$\epsilon = \exp(-\pi\gamma/\omega). \tag{7}$$

From Eqs. 4 and 5 the maximal penetration depth y_{max} follows the condition $y'(t_{max}) = 0$, so that $\omega t_{max} = \arctan(\omega/\gamma) = \arcsin(\omega/\omega_0)$ and

$$y_{max} = (v_0/\omega)\exp(-\gamma t_{max})\sin(\omega t_{max}) = (v_0/\omega_0)\exp\left[(-\gamma/\omega)\arcsin(\omega/\omega_0)\right]. \qquad (8)$$

The maximum penetration depth $y_{max}(v_0)$ is in the case of, say, steel particles much smaller than the particle diameter. Thus we check in our simulations that y_{max} is always orders of magnitude smaller than d_0.

The elasticity k in Eq. 1 is e.g. a function of the Young modulus and the Poisson ratio, which are material dependent and thus fix t_c for a given material in our simplified model. Using the theory of Hertz, a more complicated dependence of k on the impact velocity, the elasticity , and the penetration depth is found, e.g. $k \propto y^{1/2}$. In Ref. [20], the contact time of two steel spheres with diameter $d = 1.5$mm and with an impact velocity of $v_0 = 1$m/s was evaluated to $t_c \approx 4.6 \times 10^{-6}$ s. We checked for some situations that the more realistic Hertz model does not change the results [21] and thus used the simpler linear model. For a detailed discussion of different MD models and force-laws see Ref. [22].

For weak dissipation t_c is proportional to $k^{-1/2}$, so that an increase of k by a factor of 100 decreases t_c by a factor of 10. Now taking physical values for t_c leads to extremely long MD-computing times for a given simulation time. One has to insure that the time scales of the system, i.e. t_c, and of the algorithm, i.e. the integration time step t_{MD}, are well separated. Ideally one should have $t_{MD} << t_c$. The MD-simulations reported here were done with $t_{MD} < t_c/40$. Using contact times in the range $10^{-3}\text{s} < t_c < 10^{-5}\text{s}$, by choosing k according to Eq. 6, we have simulation time steps in the range $2.5 \times 10^{-3}\text{s} < t_{MD} < 2.5 \times 10^{-7}\text{s}$.

In our simulations we have as a typical set of parameters $d_0 = 1.5$mm, $k/m_{ij} = 6.67 \times 10^6\text{s}^{-2}$, $\gamma = 1.67 \times 10^3\text{s}^{-1}$ and $t_{MD} = 10^{-5}$s. These parameters lead with the above equations to $t_c = 0.97 \times 10^{-3}$ s, and $\epsilon = 0.2$, i.e. rather strong dissipation.

B. Multi particle contacts

In Refs. [20,23,24] the above defined interaction law has been tested in the case of many particles in contact at the same time. For the viscous interaction law, i.e. the linear spring-dashpot model, energy dissipation is very inefficient, i.e. the so-called "detachment effect" occurs. The time a wave needs to propagate through a system of size $l = Ld_0$ was found to be comparable to Lt_c. Thus we will measure time in units of Lt_c, and velocities in units of d_0/t_c, i.e. particle size divided by the contact time, rather corresponding to the speed of sound inside the elastic material. Thus we have the length l as the product of typical time and typical velocity.

Dividing Eq. 1 by kl we find that the dimensionless deformation x/l in a static situation, i.e. $y' = 0$, is proportional to the dimensionless elastic force $f_{el}/(kl)$. In the gravitational field the elastic force f_{el} scales with mg, where m is the mass of the pile, so that $mg \propto kl$. We tested for several situations that our results do depend rather on the ratio g/k, than on the specific values chosen for g or k.

C. Stress Tensor and Scaling

An important quantity that allows insight into the state of the system is the stress tensor σ [25,26], which we identify in the static case with

$$\sigma_{\alpha\beta}^{(i)} = (1/V^{(i)})\Sigma\ q_\alpha f_\beta, \tag{9}$$

where the indices α and β indicate the coordinates, i.e. x and z in 2D, see Fig. 1. This stress tensor is an average over all contacts of the particles within volume $V^{(i)}$, with q denoting the distance between the center of the particle and the contact point, and f denoting the force acting at the contact point. Throughout this study we average over the contacts of one particles (i) to get the stresses for one realization.

From a static configuration of "soft" particles we may now calculate the components of the stress tensor $\sigma_{xx}, \sigma_{zz}, \sigma_{xz}$, and σ_{zx} and also define $\sigma^+ = (\sigma_{xx} + \sigma_{zz})/2$, $\sigma^- = (\sigma_{xx} - \sigma_{zz})/2$, and $\sigma^* = \sigma_{xz}$. Since we neglected tangential forces the particles are torque-free and we observe only symmetric stress tensors, i.e. $\sigma_{zx} = \sigma_{xz}$. The eigenvalues of σ are thus $\sigma_{max,min} = \sigma^+ \pm \sqrt{(\sigma^-)^2 + (\sigma^*)^2}$, and the major eigenvalue is tilted by an angle

$$\phi = \arctan\left(\frac{\sigma_{max} - \sigma_{xx}}{\sigma_{xz}}\right) = \frac{\pi}{2} + \frac{1}{2}\arctan\left(\frac{2\sigma_{xz}}{\sigma_{xx} - \sigma_{zz}}\right) \tag{10}$$

from the horizontal in counter clockwise direction.

In order to find the correct scaling for the stress we assume like Liffman et al. [8,11], as a simplified example, a rigid triangle with the density ρ, the width l, the height h, and the mass $m = \rho hl/2$. Since the material is rigid, we find a constant force at the supporting surface, so that the pressure is also constant $p = mg/l = \rho gh/2$. Thus we will scale the stress by the pressure p and furtheron use the dimensionless stress

$$S = \frac{2\sigma}{\rho gh} = \frac{\sigma l}{mg} = \frac{\sigma 2a}{hmg}, \tag{11}$$

with the volume $a = hl/2$ of the triangular pile. The vertical component will be abbreviated with $V = S_{zz}$, the horizontal component with $H = S_{xx}$, and the shear component $Q = S_{xz}$. Besides the components of S we will also plot the stress tensor in its principal axis representation, i.e. for each particle we plot the scaled major principal axis along ϕ and the minor axis in the perpendicular direction.

IV. RESULTS

A. Piles with Bumpy Bottom

1. Comparison of Piles with different Slope

The first situation we address is a homogeneous pile, as assumed in Refs. [11,9]. Here we use $L_1 = 20$ particles in row $M = 1$ and create a 60^o pile. The $L_0 = 21$ particles in the lowermost row $M = 0$ are fixed with separation d_0. The particles have no horizontal contacts, so that the contact network is a diamond structure. As predicted in Refs. [11,9] the normal force at the bottom is a constant, independent from the horizontal coordinate. In Fig. 2(a) we plot the components of the dimensionless stress tensor $S(1)$ versus $X = x/l$ for the lowermost row of mobile particles, $M = 1$. The vertical component is constant, and due to the scaling used $V = 1$. We compare this result with two 30^o piles with either $L_1 = 20$ or

$L_1 = 97$ and plot again $S(1)$ vs. X for both system sizes in Fig. 2(b). For the 60^o pile the diagonal elements of S are constant, whereas for the 30^o piles we observe a plateau in the center with decreasing stresses towards the left and right ends of the pile. Our simulation results are in agreement with analogous simulations in Ref. [11], i.e. we observe no sharp edges in the stresses, where the slopes change, as predicted by the theory in Ref. [11].

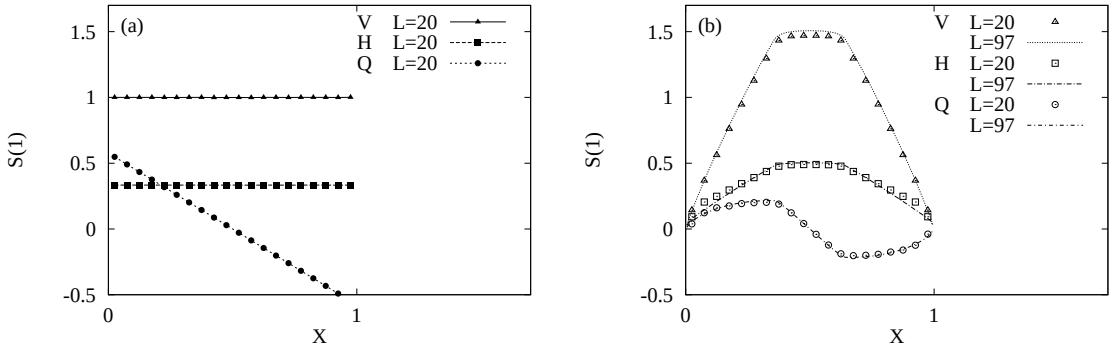

FIG. 2. Components of the dimensionless stress tensor $S(1)$ at row $M = 1$ vs. dimensionless horizontal coordinate $X = x/l$, for a pile with immobile particles at the bottom, $M = 0$. The slope of the pile is 60^o with $L_1 = 20$ in (a), and 30^o with $L_1 = 20$, or $L_1 = 97$ in (b). We indicate the vertical stress with $V = S_{zz}$, the horizontal stress with $H = S_{xx}$, and the shear stress with $Q = S_{xz}$.

From Fig. 2 we conclude that our soft particle model is able to reproduce the known analytical results of Refs. [11,9]. $V = 1$ corresponds to the constant normal stress $\sigma_{zz} = mg/l$ and thus to the normal force f_z exerted on each particle in row $M = 1$. Here $f_z = d_0\sigma_{zz} = mg/L$, with the mass of the pile $m = L(L+1)m_0/2$, and the mass of one particle m_0. Our result $f_z = (L+1)m_0g/2$ coincides with Ref. [11] [see eq.42 therein].

2. Variation of System Width for Bumpy Bottom

In this subsection we will examine the difference between the theoretical predictions for the stresses and the numerical simulations, both in Ref. [11] for the 30^o pile. The theory is based on the assumption that the contact network is a diamond lattice. Thus we perform different simulations with a 30^o pile with $L_1 = 19$ and change the contact network by increasing or decreasing the separation of the fixed particles in row $M = 0$. The centers of the particles in the lowermost row are separated by a distance $d_0(1+c)$, with the c values $c = 1/15$, 0, -1/750, and -1/150. In Fig. 3(a) and (c) we plot the vertical and horizontal components of the stress tensor, and in Fig. 3(b) and (d) we plot the contact network and the principal axis of the stress tensor respectively.

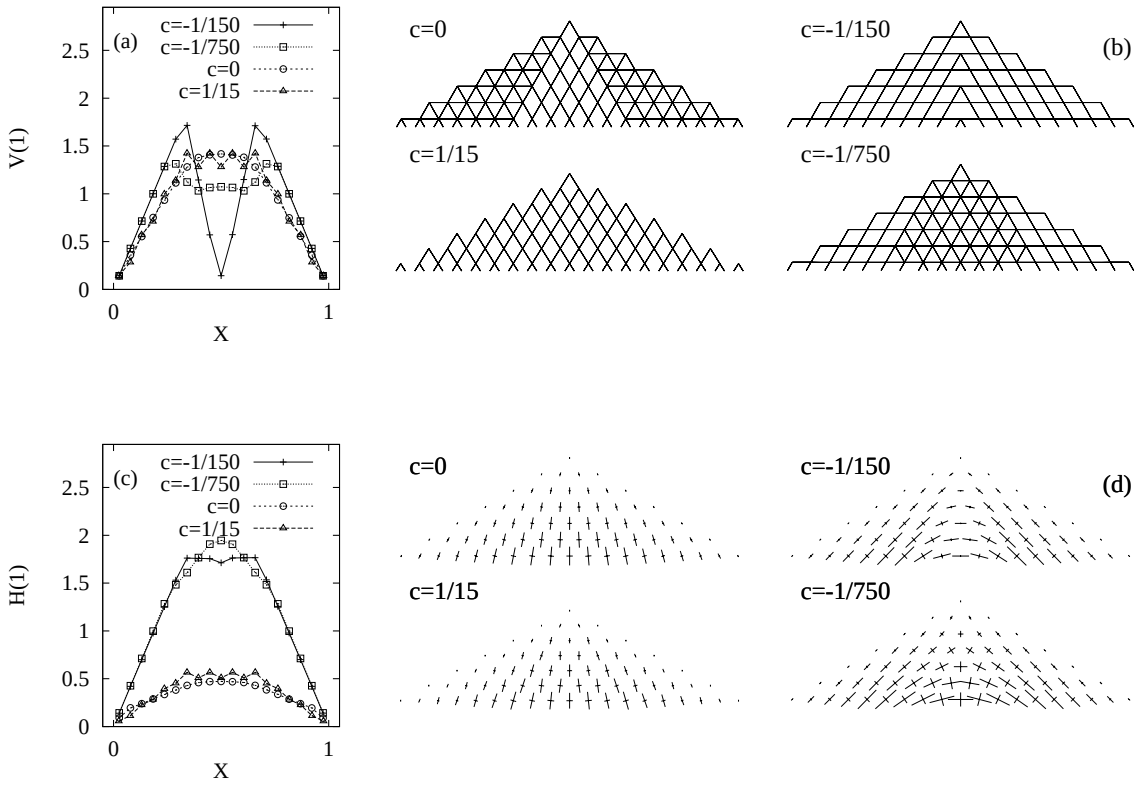

FIG. 3. (a) Vertical stress $V(1)$, in row $M = 1$, vs. X for a 30^o pile with bumpy bottom and $L_1 = 19$. The immobile particles in row $M = 0$ are separated by a distance $d_0(1 + c)$, i.e. are sqeezed together for negative c or separated for positive c. (b) The contact networks for the corresponding systems. (c) Horizontal stress $H(1)$, vs. X. (d) The principal axis of the stress tensor for the corresponding systems.

The interesting result is that the vertical stress in Fig. 3(a) has a dip for negative c values, the depth of which increases with increasing magnitude of c [11]. The horizontal stress in Fig. 3(c) is much larger for negative c as for positive c.

From Fig. 3(b) we observe that the assumption of a perfect diamond lattice for the contacts is true only for $c = 1/15$. The vertical stress $V(1)$ has a zig-zag structure that we relate to the steps at the surface of a 30^o pile. For the naively used $c = 0$ and also for small negative $c = -1/750$ we have a contact network with regions of coordination number 4 and 6, corresponding to the triangular or the diamond contact network. For sqeezed bottom particles, i.e. $c = -1/150$, the contact network is again a diamond lattice, but the orientation is tilted outwards from the center. From Fig. 3(d) we obtain arching for negative c and no arching for positive c. Seemingly, a tilted diamond lattice is neccessary for an arch to form in this situation.

In Fig. 4(a) we present for the simulations from Fig. 3 the angle $\phi(1)$, see Eq. 4 about which the major principal axis is rotated from the horizontal in counterclockwise direction. For $c < 0$ we observe a constant angle in the outer part [consistent with the fixed principal axis (FPA) theory in Ref. [16]], and a transition region in the center. We observe FPA only

for negative c when we also find arching.

In contrast, for $c \geq 0$ we observe a slow continuous variation of $\phi(1)$ over the whole pile. In Fig. 4(b) we plot the ratio of the principal axis $s = S_{min}/S_{max}$ and observe an almost constant value in the outer region of the pile, whereas in the inner part the ratio is strongly c dependent.

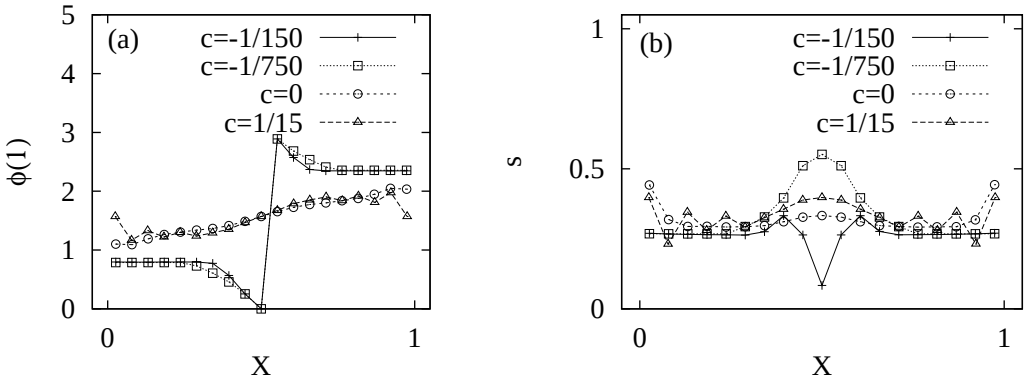

FIG. 4. (a) The angle of the major principal axis of the stress, $\phi(1)$, in row $M = 1$ vs. X, from the simulations in Fig. 3. (b) The ratio $s = S_{min}/S_{max}$ of minor to major principal axis vs. i X from the simulations in (a).

From a detailed comparison of the contact network and the stress tensor we may correlate several facts: First, the ratio of the principal axis, s, seems to determine whether the contact network is a triangular or a diamond structure, the latter with one open contact. For $c = 0$ and for $c = -1/750$ we observe the triangular contact network if s is large. Second, the direction of the diamonds is correlated to ϕ, i.e. we observe the tilted diamond lattice (for negative c) if the major axis is tilted far enough from the horizontal.

3. Removing Particles from the Pile

Now we use the pile from Fig. 2(a), i.e. 60^o with $L_1 = 20$, and examine the influence of one removed particle on the stress distribution. Here we remove the third, fifth, and seventh particle denoted with $R = 3$, 5, and 7 respectively, from the right in row $M = 7$. We relax the pile and plot the vertical normalized stress in row $M = 1$, i.e. at the bottom, in Fig. 5(a). Evidently, the formerly constant stress of the complete pile (solid line) is disturbed. We observe that the stress decreases in the region below the missing particle at $X = 0.55$, 0.65, and 0.75 for $R = 7$, 5, and 3 respectively. Interestingly, the stress is minimal when following lines parallel to the slopes of the pile, towards row M=1, starting from the vacancy. Note that following the slopes means here: following a line in the diamond contact network. The lines of contact are here tilted by 60^o from the horizontal and thus are parallel to the slopes. Going from the minimum value outwards we observe a sudden jump to the maximum value of $V(1)$. When a particle close to the center of the pile is removed, i.e. $R = 7$, for $L_7 = 14$, the stress pattern is almost symmetric to the center $X = 0.5$, whereas the pattern gets more and more asymmetric with decreasing R.

When a particle is removed, this particle can not longer transfer the stresses to its lower neighbors. Therefore the minimum stress is found when following the slopes starting from the missing particle. The stress which has not been carried by the missing particle has thus to be transferred along its right and left neighbors, what leads to the maximum stresses just outwards from the minimum stresses.

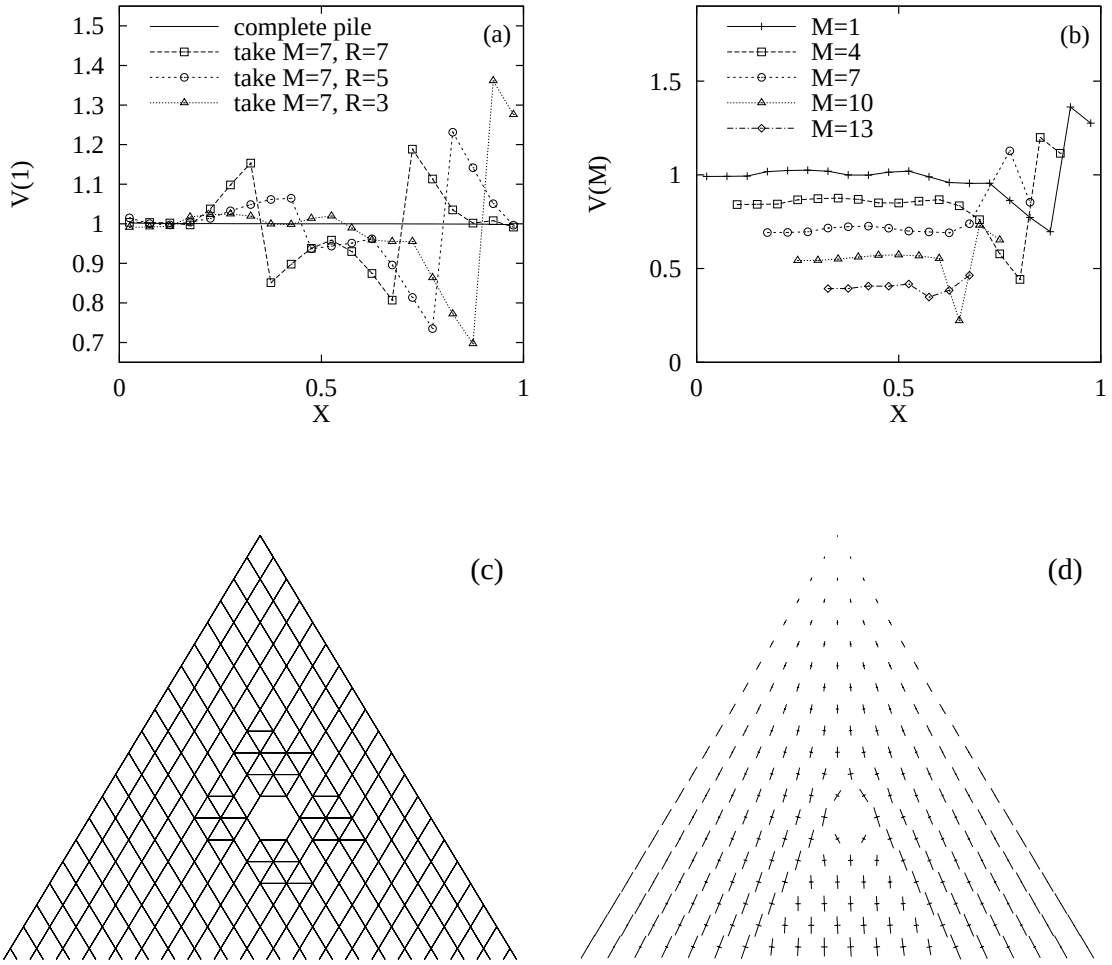

FIG. 5. (a) Vertical stress $V(1)$ in row $M = 1$ vs. X for a 60^o pile with bumpy bottom and $L_1 = 20$ (solid line). $V(1)$ is given for piles where particle $R = 7$, 5, or 3, is removed from row 7; here R counts from the right. (b) The vertical stress $V(M)$ is plotted for different rows $M = 1$, 4, 7, 10, 13, for the pile where particle 3 is removed from row 7. Note the missing symbol for $M = 7$ (circles). (c) Contact network for the situation where particle $R = 7$ is removed from row $M = 7$. (d) Principal axis of stress for the situation where particle $R = 7$ is removed from row $M = 7$.

In order to clarify this result we plot the vertical stresses V inside the pile at different heights $M = 1$, 4, 7, 10, and 13 in Fig. 5(b). With increasing M, i.e. increasing height in the pile, V decreases since the weight of the part of the pile above M decreases. Inside the pile, the stress is minimal when following the slopes downward, starting from the missing

particle. Interestingly, we observe an asymmetric stress also for $M > 7$. In Fig. 5(c) we plot the contact network for the case where particle $R = 7$ is removed from row $M = 7$. We observe an increase of the number of contacts only for the neighbors of the vacancy. From the principal axis of stress, in Fig. 5(d), we observe an arch-like structure, i.e. the stress below the vacancy is comparatively small. Furthermore, the direction of the major principal axis is almost vertical below the vacancy, and tilted outwards for the particles which carry larger stresses.

We learn by removing one particle from the pile, that stress decreases below the vacancy; however, the minimum of stress is observed when following the internal structure of the pile downwards, i.e. lines tilted by 60^o from the horizontal. Much larger stresses are observed outwards from the minima in stress, i.e. an arch-like structure is found already for one missing particle.

Note that this simulation is not in contradiction to the discussion, concerning point source terms, in Ref. [16]. Wittmer et al. discuss the effect an infinitesimally small mass element has onto the stress distribution and conclude that the (small) weight is propagated along "rays" mainly into the direction of gravity. In our case the mass removed is quite large and thus the contact network is deformed what leads to the different effects described above.

B. Pile with Smooth and Flat Bottom

In contrast to the piles with bumpy bottom, corresponding to the limit of very large friction, we model now a pile on a smooth and flat bottom, i.e. the limit of no friction. Note that this situation is stable only if the outermost particles are fixed.

1. Comparison of Piles with different Slopes

The next situation we describe is a pile on a flat, smooth bottom, i.e. the particles in row $M = 0$ are allowed to move. Only the left- and rightmost particles are fixed horizontally by the corresponding wall. In Fig. 6(a) we show the results for two 60^o piles with $L_0 = 20$ and $L_0 = 40$. The vertical component V of the stress is not constant and the horizontal component H is getting very large close to the walls, since vertical stresses are transferred into the horizontal direction and propagate directly outwards in row $M = 0$. In the case of $L_0 = 40$ we observe a relative minimum of the vertical stress in the center, $X = 0.5$.

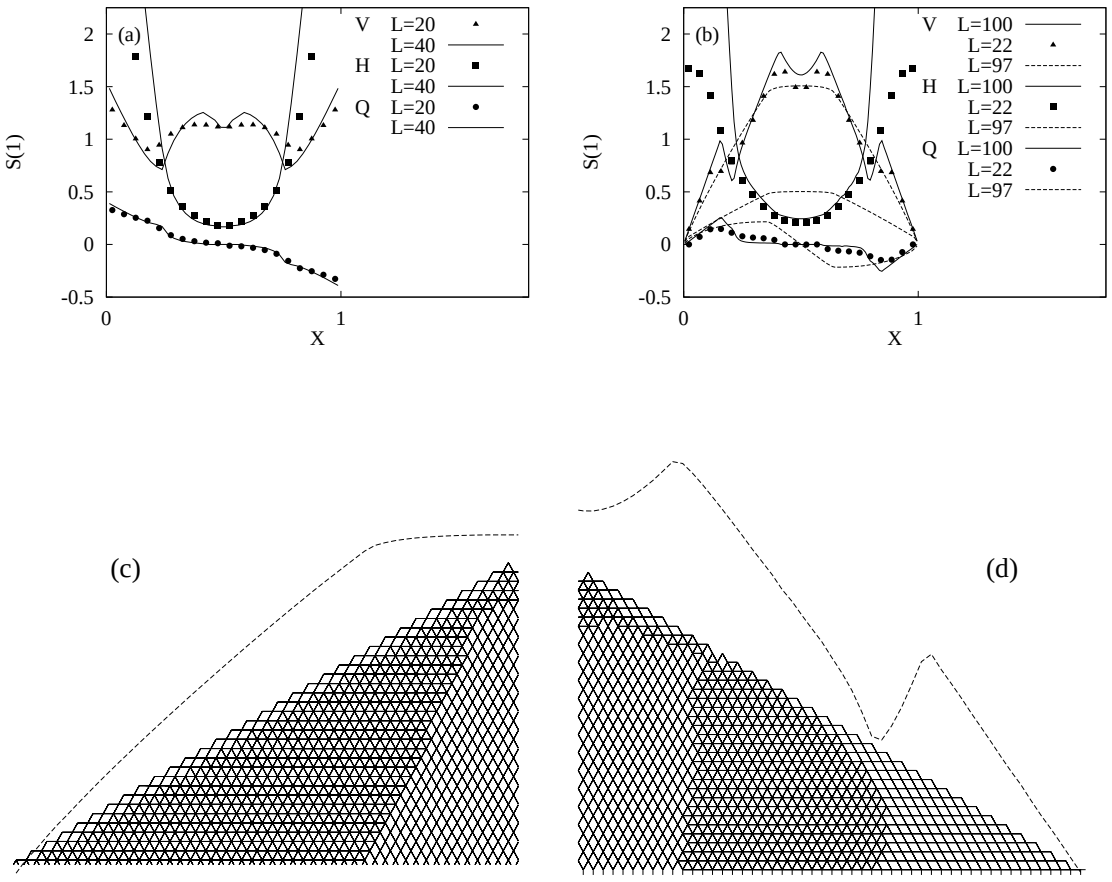

FIG. 6. Components of the dimensionless stress tensor $S(0)$ vs. dimensionless horizontal coordinate $X = x/l$ at row $M = 0$, for a pile with mobile particles at the smooth and flat bottom. We indicate the vertical stress with $V = S_{zz}$, the horizontal stress with $H = S_{xx}$, and the shear stress with $Q = S_{xz}$. (a) The slope of the pile is 60^o, and $L_0 = 20$ or $L_0 = 40$. (b) The results for 30^o and $L_0 = 100$ (solid line) or $L_0 = 22$ (symbols) are compared to the result for $L_1 = 97$ from Fig. 2(b). (c) Contact network for the left half of a 30^o pile with $L_1 = 97$ and bumpy bottom. (d) Contact network for the right half of a 30^o pile with $L_0 = 100$ and smooth, flat bottom. The dashed line in (c) and (d) gives the vertical stress V for the corresponding piles.

In Fig. 6(b) we compare the result of Fig. 2(b), i.e. $L_1 = 97$ to situations on smooth and flat bottom with $L_0 = 22$ and $L_0 = 100$. We observe fluctuations at the shoulders of the pile and again a dip in the center of the pile, $X = 0.5$. In order to find an explanation for this behavior we plot the contact networks in Figs. 6(c) and (d) for the large 30^o piles with bumpy, $L_1 = 97$ (c), and smooth, flat bottom, $L_0 = 100$ (d). The dashed lines give the vertical stress for the corresponding pile. In Fig. 6(c) we observe a contact network similar to the result in Fig. 3(b) for $c = 0$. The center triangle is arranged on a diamond lattice and the shoulders are arranged on a dense triangular lattice, i.e. the horizontal contacts are closed. Only close to the surface we have a few particles on a tilted diamond lattice. In Fig. 6(d) the situation is more complicated. We observe three regions with different structure.

First, a diamond lattice in the center, second, a dense triangular lattice in outward direction and third, the diamond lattice tilted outwards at the ends of the pile. In summary, we correlate the variations of normal stress V to the change of structure in the contact network.

2. Variation of System Width for Smooth, Flat Bottom

Now we vary the width of the system with flat, smooth bottom. Here we do not vary the box width, we just increase (or decrease) the diameters $d_1 = d_L = (1+c)d_0$ of the left- and rightmost particles in row $M = 0$. All other particles have the fixed diameter d_0 so that we change the effective width of the system. In Fig. 7 we plot the vertical stresses $V(0), V(2), V(4)$ for 30^o piles with $L_0 = 22$. We find that the dip vanishes already for slightly increasing c and relate the existence of the dip to the presence of open horizontal bonds in the center of the pile at $X = 0.5$. For decreasing c we still observe a dip structure in the pile but when c gets too small, the stress in the array of particles may get asymmetric, since the pefect triangular arangement is disturbed (see $c = -2/15$).

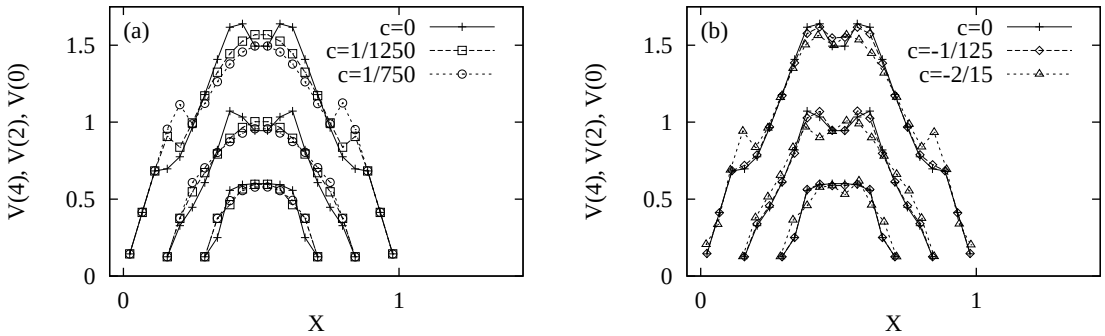

FIG. 7. Vertical stresses $V(0), V(2), V(4)$, in rows $M = 0$, 2, and 4 respectively (from top to bottom) vs. X for a 30^o pile with smooth, flat bottom and $L = 22$. The two outermost particles are fixed by vertical walls and have diameter $d = (1+c)d_0$. The inserts gives the relative change c. (a) Large boundary particles $c > 1$, and (b) small boundary particles $c < 1$.

C. Polydisperse Particles

Starting from a monodisperse 30^o pile with bumpy bottom and $L_1 = 97$, see Fig. 2(b), we change the particle size of each particle slowly to the diameter $d_i = d_0(1 + r_i)$, where r_i is a random number homogeneously distributed in the interval $[-r/2, r/2]$. We present the vertical stress in Fig. 8, for simulations with $r = 2/3000$ (a), $2/300$ (b), and $1/30$ (c). We plot the result of one run (solid line) and compare it with the monodisperse case (dashed line) and the average over 40 runs (a) or 100 runs (b) and (c) (symbols). The fluctuations in stress increase with increasing r. In fact we observe fluctuations much larger than the total stress for the monodisperse pile. With increasing r the shape of the averaged vertical stress changes in the center from a hump [see $r = 2/3000$], to a dip [see $r = 1/30$]. The averaged stress in Fig. 8(c) is similar to the stress obtained (after many averages) from a

cellular automaton model for the stress propagation in the presence of randomly opened contacts [17].

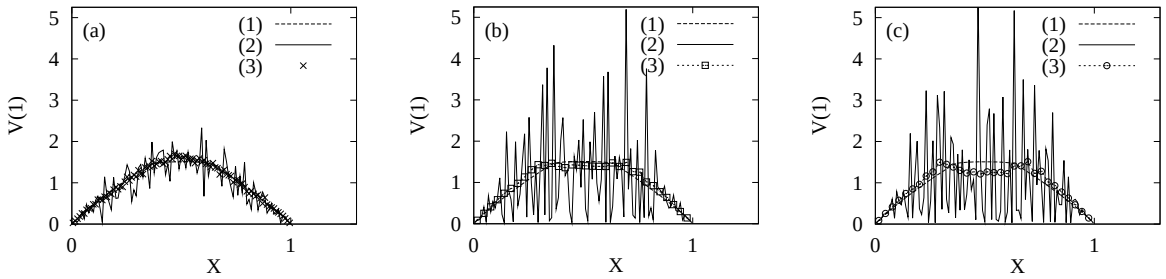

FIG. 8. Vertical stress $V(1)$, in row $M = 1$, vs. X for a 30^o pile with bumpy bottom and $L_1 = 97$. The particle diameter is homogeneously distributed in the interval $[d_0(1 - r/2), d_0(1 + r/2)]$. The values of r are $r = 2/3000$ (a), $r = 2/300$ (b), and $r = 1/30$ (c). The dashed line gives the result of Fig.2(b) with $r = 0$ and $L_1 = 97$. The solid line gives the result of one run and the symbols correspond to an average over 40 runs for (a), or 100 runs and three particles for (b) and (c).

In Fig. 9(a) we give the contact network of one run as presented in Fig. 8(c). The line thickness indicates the magnitude of forces active at a contact. In Figs. 9(b) we present a part of this contact network, and in Figs. 9(c) we plot the principal axis of the stress tensor for the same part. In Figs. 9(a) and (b) each line represents the normal direction of one contact and each particle center is thus situated at the meeting point of several lines. Note that some particles inside the pile have no contacts to their above neighbors, i.e. they are situated below an arch. Comparing the contact network (b) with the stresses in (c) one may again relate the structure of the contcat network to the angle ϕ and the ratio of the principal axis, as discussed above in Sec. IV A 2. Finally, we calculate the probability distribution P for vertical stresses V. We average only over the lowermost row $M = 1$ and also neglect the outermost particles of this row. In detail we average all particles $10 \leq i \leq 87$ [counting from the lower left end to the right] over 100 runs. Since the stress in row $M = 1$ is a function of X in the case of $r = 0$, we scale the stresses for $r > 0$ by the stresses found for $r = 0$, i.e. we use the scaled stress

$$T = V^{(r>0)}/V^{(r=0)} - \min[T], \tag{12}$$

with the minimum of all T, obtained from particles which are shielded and thus feel only their own weight, see Fig. 9. Note that this occurs frequently, even inside the pile. We checked that the probability distribution of T does not depend on the specific choice of the interval, i.e. we also averaged over a smaller interval $33 \leq i \leq 67$, or over particles in row $M = 2$ with $130 \leq i \leq 164$, and we found no difference besides fluctuations.

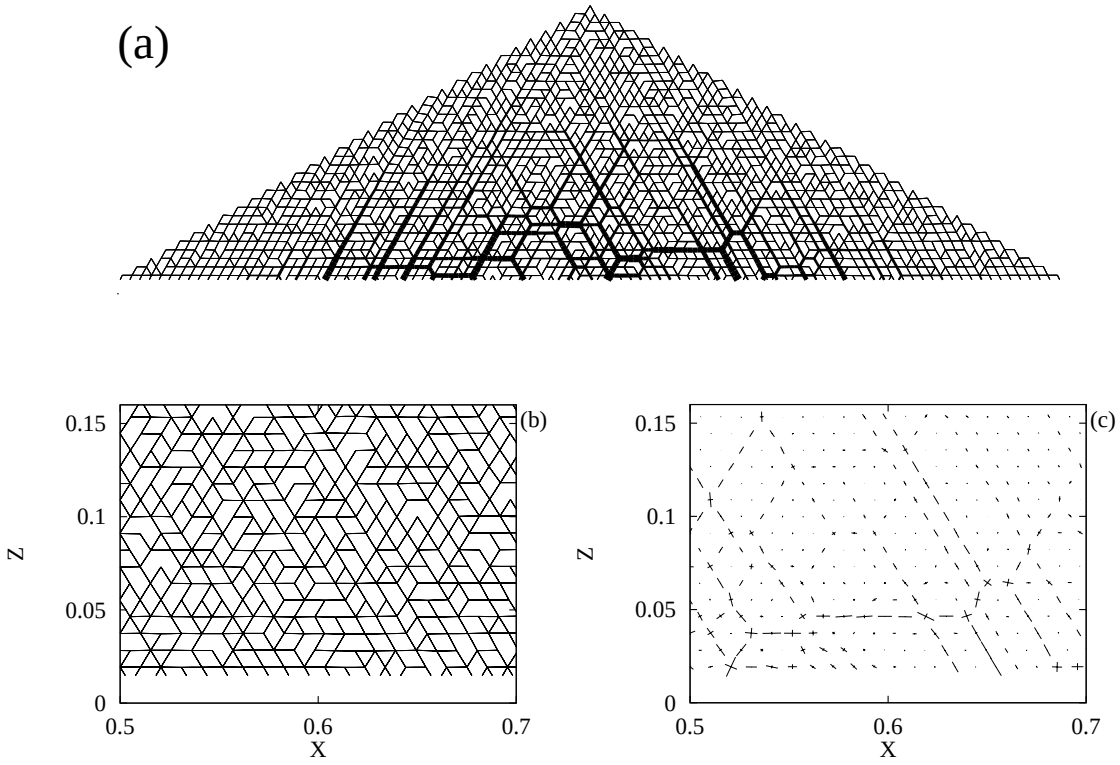

FIG. 9. (a) Contact network of one pile from Fig. 8(c). The line thickness indicates the magnitude of the contact force. (b) Part of the contact network from (a). (c) Principal axis of stress from the same simulation as in (b).

We plot the distribution function $P(T)$ in Fig. 10. The dashed line in Fig. 10(a) shows a power law for small stresses T, while the dotted line in Fig. 10(b) shows an exponential decay for large T.

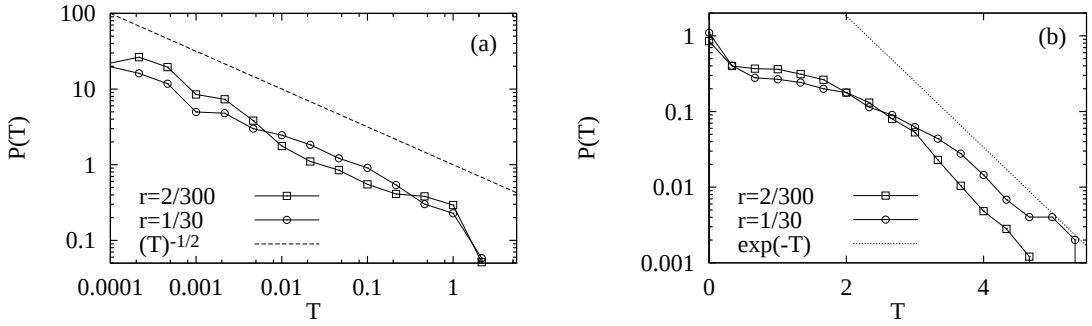

FIG. 10. (a) Double logarithmic plot of the probability distribution of small vertical stresses T in row $M = 1$. We skip 10 particles at the right and the left and average over 100 runs. see Eq. 12. (b) Log-linear plot of the probability distribution for large stresses from the same data as in (a).

Thus our results are in agreement with the theoretical predictions of Ref. [5], and the

numerical findings of Ref. [6], at least for large T, see Fig. 10(b). Note that the probabilty to find large T is greater for $r = 1/30$ than for $r = 2/300$, corresponding to stronger fluctuations. For small T we find a power law with exponent -1/2 for both values of r, see Fig. 10(a).

V. DISCUSSION AND CONCLUSION

We present simulations of static 2D piles made of almost monodisperse spheres. With this simplified model we reproduce different former theoretical predictions which were based on the assumption of a homogeneous contact network in the whole pile and perfectly rigid particles.

One fact is that arching and the so called dip in the vertical stress at the bottom are not neccessarily due to solid friction [11,14]. If the contact network varies as a function of the position in the pile we observe stresses different from the theoretical predictions based on a regular network. If we observe arching the orientation of the stress tensor is fixed, at least in the outer part, and the contact network is symmetric to the center but not translation invariant. The orientation of the major principal axis and the ratio of the two eigenvalues of the stress tensor are correlated with the structure of the contact network. We observe diamond lattices, either vertical or tilted by 60 degrees outward from the center, if the major principal stress is almost vertical or tilted outwards respectively. But if the major and minor principal axis are comparable in magnitude we observe a triangular lattice, i.e. all possible contacts closed, rather than a diamond lattice. Together with the tilted contact network, i.e. strongly tilted principal axis, we evidence in some cases arching and a small vertical stress under the center of the pile. If the contact network is tilted outwards, stresses are preferentially propagated outwards, what may be regarded as a reason for arching and for the dip.

Varying the size of the particles randomly, we find that already tiny polydispersities destroy the regular contact network. Due to the small fluctuations in particle size the particles are still positioned on a triangular lattice even when the contacts are randomly open. In the case of a random network we also find the so called stress chains, i.e. selected paths of large stresses, and the stress fluctuations are larger or of the order of the mean stress. The stress chains - or better the stress network - is also disordered. When averaging over many realizations of the stress network we get a dip in the vertical stress at the bottom if the size fluctuations are large enough. Thus we observe a similar stress distribution at the bottom as obtained by a cellular automaton model based on a random opening of contacts [17].

Since we are able to find most of the phenomenology, expected in a sandpile, already in an oversimplified regular model system without friction, we conclude that the role of the contact network (or the fabric) is eminent. Thus, we suggest to work out a formalism that accounts for the fabric in this simple framework before including the more subtle phenomena into the theory. However, friction and small polydispersity may play a different role in more general situations with physical sandpiles.

As an extension of our model we started more realistic simulations with a nonlinear Hertz contact law [21], and also with solid friction and with nonspherical particles [27]. The

effect of those more realistic interaction laws has to be elaborated and also threedimensional examinations should be performed.

ACKNOWLEDGEMENTS

We thank J. D. Goddard, H.-G. Matuttis, H. J. Herrmann, and J. J. Wittmer for helpful discussions, and acknowledge the support of the European network "Human Capital and Mobility" and of the DFG, SFB 382 (A6).

---

[1] H. M. Jaeger, S. R. Nagel, and R. P. Behringer, Physics Today **49**, 32 (1996).
[2] H. A. Janssen, Zeitschr. Vereines deutscher Ingenieure **XXXIX**, 1045 (1895).
[3] D. Trollope and B. Burman, Géotechnique **30**, 137 (1980).
[4] J. Smid and J. Novosad, I.Chem. E. Symposium Series **63**, D3/V/1 (1981).
[5] C. h. Liu *et al.*, Science **269**, 513 (1995).
[6] F. Radjai, M. Jean, J. J. Moreau, and S. Roux, Phys. Rev. Letters **77**, 274 (1996).
[7] S. Ouaguenouni and J.-N. Roux, (submitted to Europhys. Lett.).
[8] K. Liffman, D. Chan, and B. Hughes, Powder Technology **72**, 255 (1992).
[9] D. Hong, Phys. Rev. E **47**, 760 (1993).
[10] J. Huntley, Phys. Rev. E **48**, 4099 (1993).
[11] K. Liffman, D. Chan, and B. Hughes, Powder Technology **78**, 263 (1994).
[12] S. F. Edwards and R. Oakeshott, Physica D **38**, 88 (1989).
[13] J.-P. Bouchaud, M. Cates, and P. Claudin, J. Phys. I **5**, 639 (1995).
[14] S. F. Edwards and C. C. Mounfield, Physica A **226**, 25 (1996).
[15] J. Wittmer, P. Claudin, M. Cates, and J.-P. Bouchaud, Nature **382**, 336 (1996).
[16] J. Wittmer, M. Cates, and P. Claudin, J. Phys. I **7**, 39 (1996).
[17] J. Hemmingsson, H. J. Herrmann, and S. Roux, J. Phys. I **7**, 291 (1997).
[18] P. A. Cundall and O. D. L. Strack, Géotechnique **29**, 47 (1979).
[19] M. P. Allen and D. J. Tildesley, *Computer Simulation of Liquids* (Oxford University Press, Oxford, 1987).
[20] S. Luding *et al.*, Phys. Rev. E **50**, 4113 (1994).
[21] S. Luding and H.-G. Matuttis, in *Friction, Arching and Contact Dynamics*, edited by D. E. Wolf and P. Grassberger (World Scientific, Singapore, 1997).
[22] J. Schäfer, S. Dippel, and D. Wolf, J.Phys. I France **6**, 5 (1996).
[23] S. Luding *et al.*, Phys. Rev. E **50**, R1762 (1994).
[24] S. Luding *et al.*, in *Fractal Aspects of Materials* (Materials Research Society, Symposium Proceedings, Pittsburgh, Pennsylvania, 1995), Vol. 367, p. 495.
[25] J. D. Goddard, in *Recent Developments in Structered Continua. Pitman Research Notes in Mathematics No. 143*, edited by D. DeKee and P. N. Kaloni (Longman/J. Wiley, New York, 1986), p. 179.
[26] R. Bathurst and L. Rothenburg, J. Appl. Mech. **55**, 17 (1988).

[27] H.-G. Matuttis and S. Luding, in *Friction, Arching and Contact Dynamics*, edited by D. E. Wolf and P. Grassberger (World Scientific, Singapore, 1997).